

Photocatalytic and antibacterial activities of eco-friendly green synthesized ZnO and NiO nanoparticles

K. C. Lalithambika¹ · A. Thayumanavan¹ · K. Ravichandran² · S. Sriram¹

Received: 18 August 2016 / Accepted: 1 October 2016 / Published online: 5 October 2016
© Springer Science+Business Media New York 2016

Abstract ZnO and NiO nanopowders are prepared using a simple, cost-effective and eco-friendly green soft chemical method. The XRD studies shows that the prepared powders have high crystallinity with an average crystallite size of 35 and 30 nm, respectively. The EDX study confirms the presence of elements the Zn, Ni and O. Test to find the photocatalytic of ZnO and NiO nanopowders for the degradation of MB dye is performed under visible light. The results reveal that the photocatalytic efficiency of ZnO nanopowders is higher than that of NiO nanopowders. From the antibacterial studies, it is found that the prepared ZnO nanopowder exhibits higher antibacterial efficiency against *Escherichia coli* and *Staphylococcus aureus* bacteria than NiO nanopowders. The binding affinity of the bacterial strains with the prepared nanoparticles has been calculated by performing a molecular dynamics simulation and the results are found to be matched well with the experimental studies.

1 Introduction

Nanostructured materials are extensively studied owing to their potential applications in various fields which include medical, photovoltaic and optoelectronics [1–6]. Several

forms of nanostructures such as nanotubes [7, 8], nano rods [9, 10] and nano wires [11–13], are prepared extensively for various applications due to their large surface to volume ratio. Among the various nano structured materials, transition metal oxide based nano materials have attracted the material scientists because of their structure related properties and in particular their *3d* electronic configuration [14–16]. The preparation methods of the transition metal oxide nano particles play an important role in determining their structural and electronic properties as well as their applications. Transition metal oxide nano particles are prepared by several methods such as solgel [17, 18], solid state reaction [19] and co-precipitation [15, 20] etc. One of the simplest and cost-effective methods to produce transition metal oxide nano particles is green synthesis [21–23]. This is the most eco-friendly and non-toxic method which has several advantages over other methods such as simplicity, low operative temperature and low-cost. In this method, nanoparticles are prepared using naturally available plant extracts which are used as capping and reducing agents for the synthesis of the transition metal oxide nano particles. The present study focuses the synthesis of two transition metal oxides namely zinc oxide (ZnO) and nickel oxide (NiO) nano particles using the eco-friendly green synthesis method. The prepared ZnO and NiO nano particles are characterized using XRD, SEM, EDX and FTIR analysis. In addition, antibacterial activity of the synthesized ZnO and NiO nano particles against two bacterial strains *Escherichia coli* and *Staphylococcus aureus* are studied. As binding ability of the antibacterial agent with the bacteria plays an important role in deforming the antibacterial efficiency of the material, a molecular dynamics simulation is performed to confirm the binding affinity of the nanoparticles with the bacterial strains.

✉ S. Sriram
sukansriram@gmail.com

¹ Department of Physics, School of Electrical and Electronics Engineering, SASTRA University, Thanjavur, Tamilnadu 613401, India

² PG and Research Department of Physics, AVVM Sri Pushpam College (Autonomous), Poondi, Thanjavur, Tamilnadu 613503, India

2 Experimental details

2.1 Preparation of ZnO and NiO nanoparticles

Preparation of ZnO and NiO nanoparticles via green synthesis method is a twofold process as described below:

2.1.1 Preparation of leaf extract

The fresh neem (*Azadirachta indica*) leaves were collected from SASTRA University, Tirumalisamudram, Thanjavur, India first. They were thoroughly washed several times using distilled water. These washed leaves were then dried under a sunshade to eliminate the moisture totally. Using a mechanical grinder, the leaves were powdered and then stored in an airtight container. To make the neem powder solution, 100 ml of distilled water was taken in a beaker and 5 g of powdered neem plant leaves were added. They are heated to a temperature of 60 °C for 60 min with constant stirring using a magnetic stirrer. Then it was cooled down to room temperature. The extract prepared was filtered first using a normal filter paper and the leafy materials were filtered out. Then it was filtrated using Whatman No. 1 filter paper to obtain a clear solution. This *Azadirachta indica* leaf extract was used as the reducing agent for the synthesis of ZnO and NiO nanoparticles. The excess extract obtained can be stored at 4 °C for future works.

2.1.2 Synthesis of ZnO and NiO nanopowders

For ZnO nanoparticle preparation, 50 ml solution of neem leaf extract was taken in a beaker and 0.2 M of zinc acetate (purity 99 %) was added to it and the solution was heated to 60 °C under constant stirring. The stirring process is continued until a deep yellow color paste was obtained. Then it was transferred to a ceramic crucible and dried completely in open atmosphere. The final sample was powdered using a laboratory Mortar and Pestle to reduce the dimensions and to obtain pale yellow ZnO nanoparticles. Then it was heated at a temperature of 400 °C for 2 h.

For the preparation of NiO nano particles, similar procedure is followed with 0.2 M of Nickel acetate (purity 99 %) instead of zinc acetate. In this case, the final product (NiO nanoparticles) was in black color.

2.2 Characterization of green synthesized ZnO and NiO nanopowders

The crystalline structures of the synthesized ZnO and NiO nanopowders were analysed using X-ray powder diffraction method (PANalytical-PW 340/60X⁺pert PRO) with Cu-K_α (1.5406 Å) radiation. The surface morphology

(SEM) and the elemental composition analysis (EDX) were carried out using scanning electron microscope (SEM–HITACHIS-3000H). The fourier transform infrared (FTIR) spectra were recorded in the range of 4000–400 cm⁻¹ using FTIR spectrometer (Spectrum 100, Perkin Elmer, USA). The electrical conductivity measurements for the prepared nanopowders were carried out using KOKUYO KC-605 LCR meter at a frequency of 10 kHz.

2.3 Photocatalytic test

The photocatalytic degradation test for the ZnO and NiO nanopowders samples was evaluated for the photodegradation of Methylene Blue (MB) dye in aqueous solution under visible light irradiation using Xe arc (300 W) lamp. 50 mg of the prepared nanopowders was dissolved in 150 mL of MB aqueous solution (1×10^{-5} M) separately and sonicated for 45 min in dark in order to reach adsorption–desorption equilibrium. Under ambient conditions, the solutions were exposed to visible light for 60 min. For every 15 min the reaction solutions were sampled, centrifuged and filtered to remove the photocatalyst. The degradation efficiency of MB is calculated for both the samples by recording the absorption spectra of the test dye and finding the absorption intensity at the characteristic absorption peak appears at 664 nm using a UV–Vis spectrophotometer (Systronics 2002).

2.4 Evaluation of antibacterial activity

The antibacterial activity of the green synthesized ZnO and NiO nanopowders was performed using agar well diffusion method against *Escherichia Coli* (*E. coli*) a gram negative bacteria and *Staphylococcus aureus* (*S. aureus*) a gram positive bacteria. The nutrient agar medium was used for the bacterial growth. Then this medium is poured onto the petri plates and after solidification using a sterile cotton swab, fresh cultures of the bacteria were spread over the plates. The wells were punched onto these agar plates using a cork borer and these wells are loaded with 200 µg/mL of stock solution. After these, the plates were incubated at 37 °C for 24 h and the plates were observed for the inhibition zones around the well. The zone of inhibition was recorded by measuring the diameter of the inhibition zone around the well in mm. Ciprofloxacin was used as a standard antibiotic for comparison.

3 Results and discussion

3.1 Structural characteristics

Figure 1 shows the XRD patterns of ZnO and NiO nanopowders prepared using green synthesis method. In the case of ZnO nanopowders, the observed diffraction

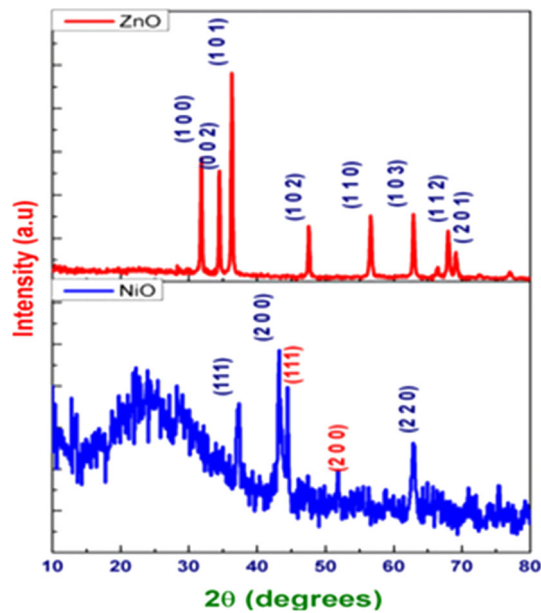


Fig. 1 XRD patterns of ZnO and NiO nanopowders

peaks are related to (110), (002), (101), (102), (110), (103), (112) and (201) lattice planes of the hexagonal wurtzite structure of ZnO (JCPDS card no 36-1451). The first three strongest peaks are found to be lattice planes having hkl values (101), (100) and (002). The observed XRD profile of ZnO nanopowder shows that the particles are well crystallized and there is no evidence for any other secondary phases. The preferential growth of the ZnO nanopowders is found to be along (101) plane. In the case of NiO nanopowder, the diffraction peaks are observed for (111), (200) and (220) lattice planes of fcc NiO (JCPDS card no 04-835). Two unmatched diffraction peaks around $2\theta = 44.4^\circ$ and $2\theta = 53^\circ$ are also found which are associated with (111) and (200) lattice planes of transition metal Ni fcc structure (JCPDS card no 04-850). This secondary phase confirms that the grown particles are in mixed phase with Ni as well as NiO nanopowders.

The crystallite size (D) of the ZnO and NiO nanopowders were calculated using Scherrer's formula [24]

$$D = \frac{0.9\lambda}{\beta \cos \theta} \quad (1)$$

where λ is the wavelength of Cu- K_α radiation (1.5406 Å), θ is the Bragg's angle and β is the full width at half maximum (FWHM).

The lattice constants 'a' and 'c' for ZnO nanopowders and 'a' for the NiO nanopowders were calculated using the formulae [25, 26]

$$\frac{1}{d^2} = \frac{4}{3} \frac{(h^2 + hk + k^2)}{a^2} + \frac{l^2}{c^2} \quad (2)$$

Table 1 Structural parameters of ZnO and NiO nanopowders

Sample	Crystallite size (nm)	Lattice constant	
		a (Å)	c (Å)
ZnO	35	3.252	5.2036
NiO	30	4.175	–

$$a = d(h^2 + k^2 + l^2)^{1/2} \quad (3)$$

respectively, where d is the inter planar spacing and h , k and l are the Miller indices. The calculated structure parameters are shown in Table 1.

3.2 Morphological studies

The SEM images of ZnO and NiO nanopowder samples are shown in the Fig. 2. From the figure it is seen that the prepared ZnO nanopowders exhibit agglomeration of spherical grains. However, in the case of NiO nanopowders, well defined minute spherical grains are seen. Figure 3 represents the elemental composition analysis (EDX) spectra of ZnO and NiO nanopowders. The figure confirms the presence of the expected elements in the corresponding nanopowders.

3.3 FTIR studies

Figure 4 shows the FTIR spectra of ZnO and NiO nanopowders prepared using green chemical method. In the case of ZnO nanopowder, a strong peak is observed near 3400 cm^{-1} which is the characteristic peak of the hydroxyl group formed due the H_2O molecule in the compound. A broad band appears around 1400 cm^{-1} is due to asymmetric and symmetric C=O stretching. The sharp peak appearing around 530 cm^{-1} is associated with Z–O stretching vibrations. However, for the NiO nanopowders, a sharp peak around 1600 cm^{-1} correspond to the hydroxyl group is observed.

3.4 Electrical studies

To study the electrical conductivity of the prepared ZnO and NiO nanopowder samples, the samples were pelletized using a hydraulic pelletizer. The average thickness of ZnO and NiO nano pellets is 1.6 mm. To measure the electrical conductivity, the pellets were connected with electrodes of the LCR meter using silver paste. The LCR frequency was set to 10 kHz. The measured electrical conductivity of ZnO and NiO samples were 1.118×10^{-8} and $1.58 \times 10^{-8} \text{ } \Omega^{-1} \text{ m}^{-1}$, respectively.

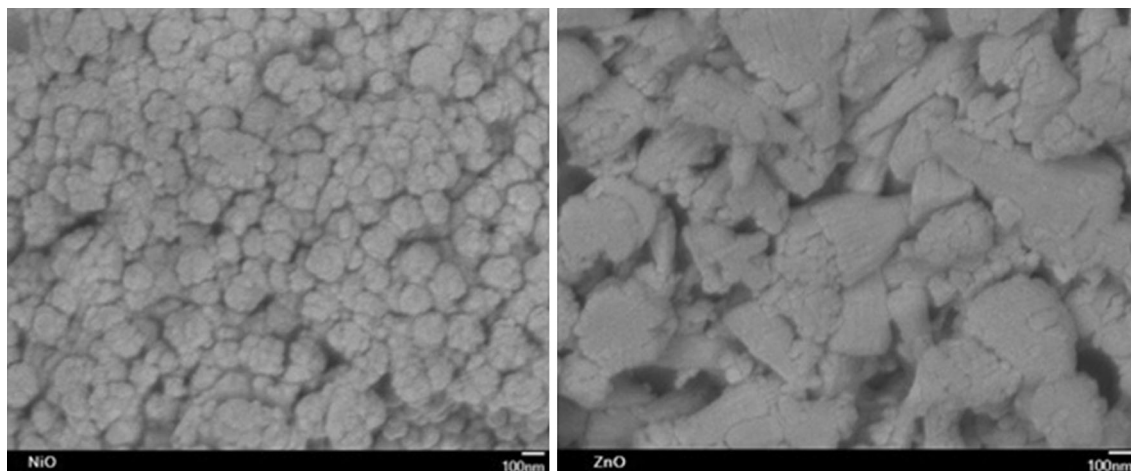


Fig. 2 SEM images of ZnO and NiO nanopowders synthesized by green method

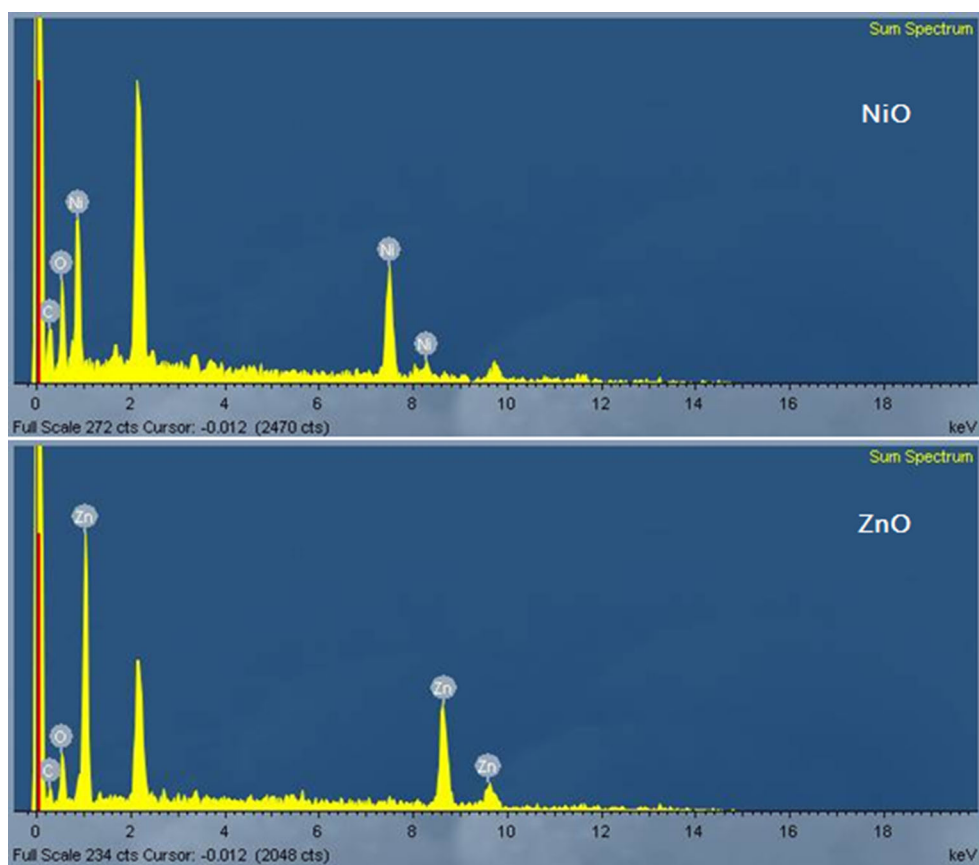


Fig. 3 Elemental composition analysis of ZnO and NiO nanopowders synthesized by green method

3.5 Evaluation of MB dye degradation

The photocatalytic activity of ZnO and NiO nanopowders are evaluated through MB dye degradation under visible light irradiation. Figure 5 illustrates the absorption spectra of MB solution with the prepared photocatalyst at different time intervals. From the spectra, it is found that the

intensity of the characteristic absorption peak of MB dye at 663 nm decreases gradually with the increase in irradiation time for both the samples. This decrease in intensity shows the photocatalytic degradation of dye molecules in the aqueous solution. The photocatalytic degradation efficiency was calculated using the formula [27]

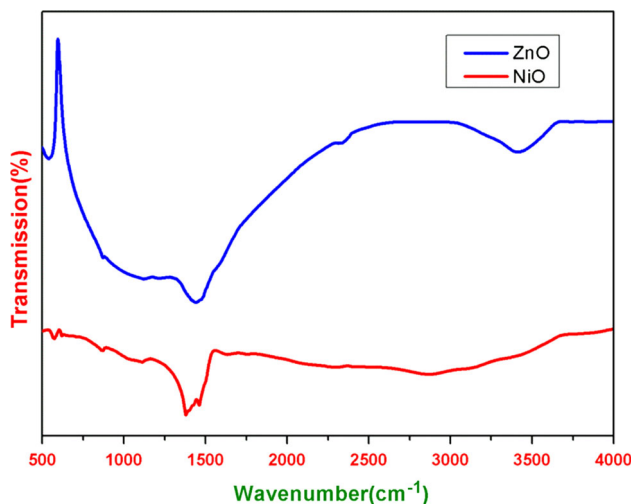


Fig. 4 FTIR spectra of ZnO and NiO nanopowders

$$\eta = (C_0 - C_t)/C_0 \times 100 = (A_0 - A)/A_0 \times 100 \quad (4)$$

where C_0 is the initial concentration of the tested dye and C_t is the concentration at the time of irradiation 't'. A_0 and A are the corresponding absorbance values. The calculated degradation efficiency after 60 min of visible light irradiation is 79.5 and 88.8 % for NiO and ZnO samples, respectively.

The above results reveal that ZnO exhibits higher efficiency compared to NiO sample against MB dye. This increase in efficiency may be due to the following aspects (1) effective separation of the photogenerated charge carriers and an increased charge carrier lifetime (2) large content of oxygen vacancies or defects which act as trapping centres for the photogenerated electrons. These oxygen vacancies can also promote absorption of O_2 that are converted into super oxide radicals ($\cdot O_2^-$). These super oxide radicals are active to produce other radicals such as OH^- , H_2O_2 to degrade the organic dye molecules.

The photocatalytic reactions follow pseudo-first-order reaction. Its kinetics can be expressed using $\ln(C_0/C_t) = k_{app} \times t$, where k_{app} is the apparent reaction rate constant. Reaction rate constants are estimated as 0.036351 and 0.026268 min^{-1} for ZnO and NiO nanopowders, respectively (in Fig. 6). This result indicate that the rate constant of ZnO is marginally larger than that of NiO sample.

3.6 Anti bacterial activity

The antibacterial activity of ZnO and NiO nanoparticles produced by green synthesis method is investigated using agar well diffusion method against *E. coli* and *S. aureus* bacteria. Figure 7 shows the zone of inhibition around the bacterial strain for ZnO and NiO nanoparticles. The diameters of the zones of inhibition obtained from the test are listed in Table 2. The results show that, the antibacterial efficacy of the ZnO nanoparticles prepared in this study is higher than that of NiO nanoparticles for both the tested bacteria. It is noted that when compared with the standard antibacterial agent (Ciprofloxacin), the prepared ZnO and NiO nanopowders exhibit antibacterial efficiency about 83 and 96 % against *S. aureus* bacteria whereas the antibacterial efficiency of these two synthesized materials is slightly lesser in the case of *E. coli* (56 and 73 % for NiO and ZnO). The reason for the decrease in the antibacterial efficacy of the prepared nanopowders against *E. coli* may be due its gram negative nature. It is well known that gram negative bacteria consist of multiple cell walls compared to gram positive bacteria (*S. aureus*).

3.7 Molecular simulation

To perform the molecular modelling for finding out the binding affinity of NiO and ZnO nano particles with the two bacterial strains, two small clusters of NiO and ZnO were constructed and converted into pdb (Protein data

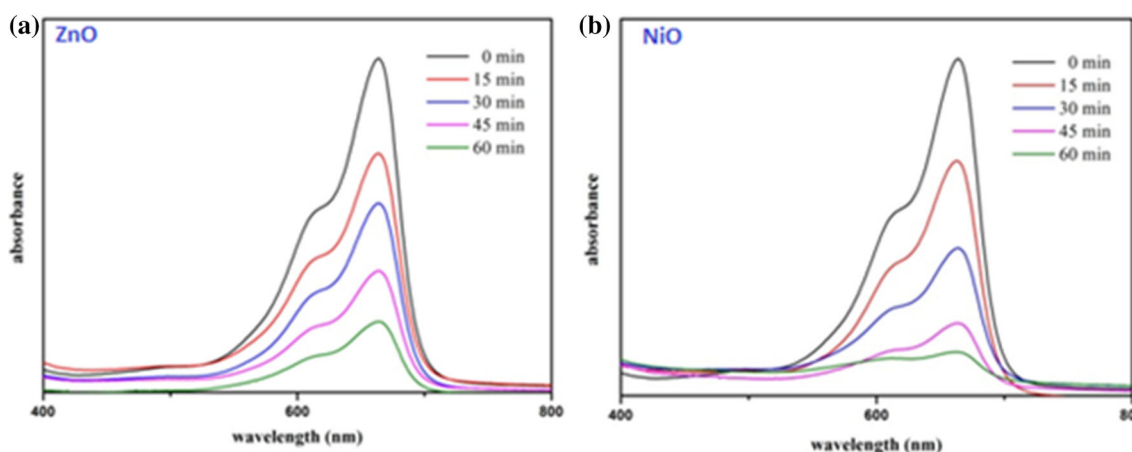


Fig. 5 Absorption spectra of MB aqueous solution under visible light with **a** ZnO and **b** NiO nanopowders

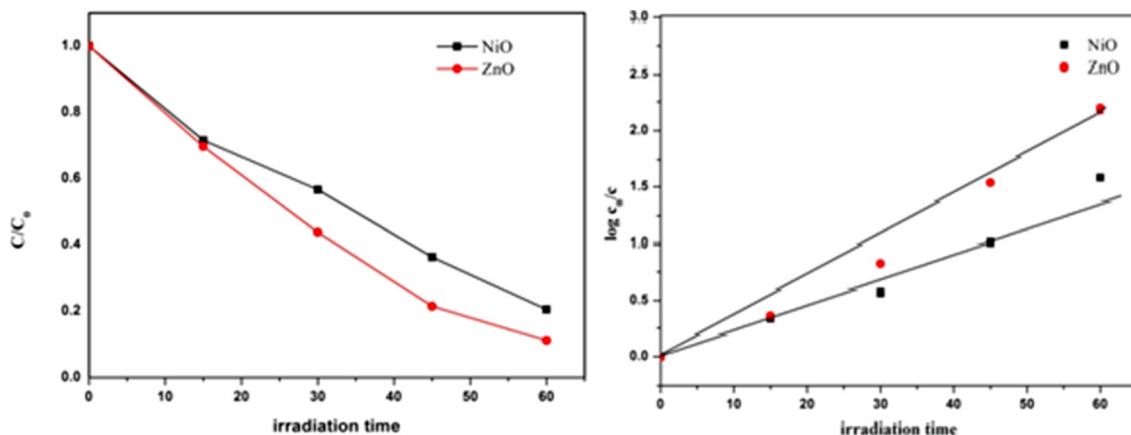


Fig. 6 MB concentration changes with time of ZnO and NiO nanopowders

Fig. 7 Antibacterial activity of ZnO and NiO nanopowders against *E. coli* and *S. aureus*

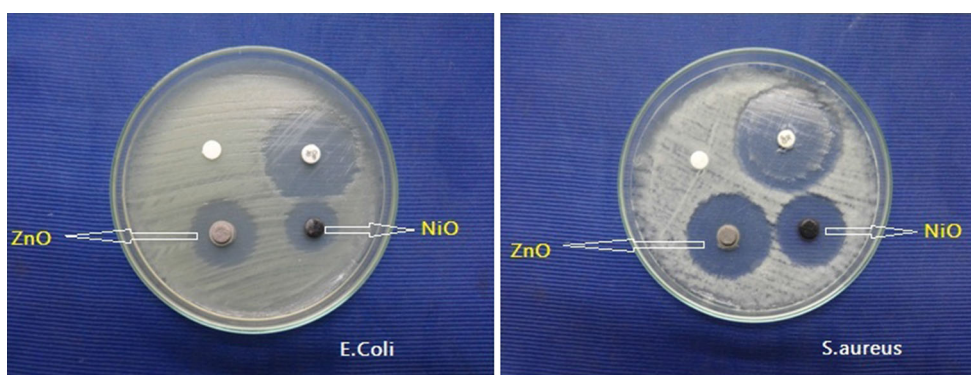


Table 2 Assay of antibacterial activity

S. No.	Bacteria	Zone of inhibition (mm in diameter)			
		Control	Standard ^a	NiO	ZnO
1	<i>Staphylococcus aureus</i>	–	31	26	30
2	<i>Escherichia coli</i>	–	30	17	22

^a Ciprofloxacin

bank) file format. The pdb files of bacterial strains of *E. coli* and *S. aureus* were taken in order to find out the binding affinity with the corresponding nano particles. These initial structures for the binding affinity simulation were performed by using docking simulations with Auto-Dock Vina software [28]. Usually the docking simulations were performed to identify the more affine state of a ligand with the protein using an energy based scoring function [28]. The calculated binding affinity of the nanoparticles with the corresponding bacterial protein is shown in Table 3. From the results it is clear that the ZnO nanoparticles have more affinity than NiO nanoparticles with both *E. coli* and *S. aureus* bacterial strains. This result validates the experimental results obtained in this study, which shows that ZnO is more reactive than the NiO nanoparticles with the tested bacterial strains.

Table 3 Binding affinity of ZnO and NiO nanoparticles with bacterial strains

S. No.	Combination	Binding affinity (Kcal/mol)
1	<i>E. coli</i> + NiO	–11.5
2	<i>S. aureus</i> +NiO	–10.5
3	<i>E. coli</i> + ZnO	–11.9
4	<i>S. aureus</i> + ZnO	–10.5

4 Conclusion

ZnO and NiO nanopowders were synthesized by a cost effective and eco friendly green synthesise method. It is noted that the synthesized ZnO and NiO nanopowders have high crystalline quality with an average crystallite size of

35 and 30 nm, respectively. The elemental composition analysis confirms the presence of the Zn, Ni and O components. The results of photodegradation of Methylene Blue (MB) dye tests show that the photocatalytic efficiency of ZnO nanopowders is higher than that of NiO nanopowders. The antibacterial studies show that between the prepared ZnO and NiO nanopowders, ZnO nanopowder exhibits higher sensitivity against both the bacterial strains of *E. coli* and *S. aureus*. A confirmation study is also done using molecular dynamics simulation. The results obtained from the molecular dynamics simulation is agreed well with the obtained experimental results.

References

1. I. Brigger, C. Dubernet, P. Couvreur, *Adv. Drug Deliv. Rev.* **64**, 24 (2012)
2. P.C. Nagajyothi, T.V.M. Sreekanth, C.O. Tettey, Y.I. Jun, S.H. Mook, *Bioorg. Med. Chem. Lett.* **24**, 4298 (2014)
3. M.M. Rashad, A.E. Shalan, M. Lira-Cantú, M.S.A. Abdel-Mottaleb, *Appl. Nanosci.* **3**, 167 (2013)
4. N. Kalfagiannis, P.G. Karagiannidis, C. Pitsalidis, N.T. Panagiotopoulos, C. Gravalidis, S. Kassavetis, P. Patsalas, S. Logothetidis, *Sol. Energy Mater. Sol. Cells* **104**, 165 (2012)
5. M. Notarianni, K. Vernon, A. Chou, M. Aljada, J. Liu, N. Motta, *Sol. Energy* **106**, 23 (2014)
6. N. Suganthi, K. Pushpanathan, *J. Mater. Sci: Mater. Electron.* **27**, 10089 (2016)
7. C. Wang, B. Mao, E. Wang, Z. Kang, C. Tian, *Solid State Commun.* **141**, 620 (2007)
8. H.B. Lu, L. Liao, H. Li, Y. Tian, D.F. Wang, J.C. Li, Q. Fu, B.P. Zhu, Y. Wu, *Mater. Lett.* **62**, 3928 (2008)
9. M. Raja, N. Muthukumarasamy, D. Velauthapillai, R. Balasundaraprabhu, *Superlattices Microstruct.* **72**, 102 (2014)
10. S. Lakehal, S. Achour, C. Ferrari, E. Buffani, F. Rossi, F. Fabri, *Superlattices Microstruct.* **72**, 253 (2014)
11. L. Wu, Y. Wu, H. Wei, Y. Shi, C. Hu, *Mater. Lett.* **58**, 2700 (2004)
12. G. Singh, A.T.J. Van Helvoort, S. Bandyopadhyay, S. Volden, J.P. Andreassen, W.R. Glomm, *Appl. Surf. Sci.* **311**, 780 (2014)
13. J. Cui, *Mater. Charact.* **64**, 43 (2012)
14. S.C. Kulkarni, D.S. Patil, *J. Mater. Sci. Mater. Electron.* **27**, 3731 (2016)
15. H. Zhang, J.-L. Cao, G.-S. Shao, Z.-Y. Yuan, *J. Mater. Chem.* **19**, 6097 (2009)
16. D. Bresser, F. Mueller, M. Fiedler, R. Kloepsch, D. Baither, M. Winter, E. Paillard, S. Passerini, *Chem. Mater.* **25**, 4977 (2013)
17. M. Vafaei, M.S. Ghamsari, *Mater. Lett.* **61**, 3265 (2007)
18. M. Ristic, S. Music, M. Ivanda, S. Popovic, *J. Alloys Compd.* **397**, 4 (2005)
19. C.-J. Chen, R.-K. Chiang, *Dalt. Trans.* **40**, 880 (2011)
20. S.S.P. Sultana, D.H.V. Kishore, M. Kuniyil, M. Khan, A. Alwarthan, K.R.S. Prasad, J.P. Labis, S.F. Adil, *Arab. J. Chem.* **8**, 766 (2015)
21. M.S. Al-Ruqeishi, T. Mohiuddin, L.K. Al-Saadi, *Arab. J. Chem.* (2016). doi:10.1016/j.arabjc.2016.04.003
22. S.S.M. Hassan, H.I. Abdel-Shafy, M.S.M. Mansour, *Arab. J. Chem.* (2016). doi:10.1016/j.arabjc.2016.04.009
23. S. Venkateswarlu, B. NateshKumar, C.H. Prasad, P. Venkateswarlu, N.V.V. Jyothi, *Physica B Condens Matter.* **449**, 67 (2014)
24. A.T. Ravichandran, K.C.S. Pushpa, K. Ravichandran, K. Karthika, B.M. Nagabhushana, S. Mantha, K. Swaminathan, *Superlattices Microstruct.* **75**, 533 (2014)
25. R. Anandhi, R. Mohan, K. Swaminathan, K. Ravichandran, *Superlattices Microstruct.* **51**, 680 (2012)
26. S. Sriram, A. Thayumanavan, K. Ravichandran, *Surf. Eng.* **32**, 207 (2016)
27. K. Ravichandran, N. Chidambaram, S. Gobalakrishnan, *J. Phys. Chem. Solids* **93**, 82 (2016)
28. Z. Faghieh, M. Fereidoonzhad, S.M.H. Tabaei, Z. Rezaei, A.R. Zolghadr, *Chem. Phys.* **459**, 31 (2015)